Title

The derivative of a waveguide acoustic field with respect to a three-dimensional sound speed perturbation

Journal

The Journal of the Acoustical Society of America, 115(6)

ISSN

0001-4966

Author

Thode, Aaron

Publication Date

2004-06-01

DOI

10.1121/1.1736651

Peer reviewed

The derivative of a waveguide acoustic field with respect to a three-dimensional sound speed perturbation[a)]

Aaron Thode[b)]
Marine Physical Laboratory, Scripps Institution of Oceanography, San Diego, California 92093-0205

(Received 11 July 2003; accepted for publication 15 March 2004)

Semianalytic expressions are derived for the first-order derivative of a pressure field in a laterally homogeneous waveguide, with respect to an arbitrary three-dimensional refractive index perturbation in either the water column or ocean bottom. These expressions for the ''environmental derivative,'' derived using an adjoint method, require a three-dimensional spatial correlation between two Green's functions, weighted by an environmental parameter basis function, with the Green's functions expressed in terms of normal modes. When a particular set of orthogonal spatial basis functions is chosen, the three-dimensional spatial integral can be converted into a set of one-dimensional integrations over depth and azimuth. The use of the orthogonal basis permits environmental derivatives to be computed for an arbitrary sound-speed perturbation. To illustrate the formulas, a simple sensitivity study is presented that explores under what circumstances three-dimensional plane-wave and cylindrical perturbations produce non-negligible horizontal refraction effects, for a fixed source/receiver geometry. Other potential applications of these formulas include benchmarking three-dimensional propagation codes, and computing Cramer–Rao bounds for three-dimensional environmental parameter estimates, including internal wave components. [DOI: 10.1121/1.1736651]

PACS numbers: 43.30.Pc; 43.30.Bp [WLS] Pages: 2824–2833

I. INTRODUCTION

The full-field inversion of ocean acoustic data for water-column sound speed and bottom geoacoustic properties requires adequate understanding of the sensitivity of a modeled acoustic field to various kinds of environmental perturbations. If the field is relatively insensitive to a particular parameter, then attempts to invert the parameter will yield estimates with large variances and biases for a given signal-to-additive-noise ratio (SANR). One quantitative measure of this sensitivity is the derivative of an acoustic field with respect to an environmental parameter, or ''environmental pressure derivative.'' More rigorous measures of the minimum possible variance and bias of a parameter estimate, including the Cramer–Rao lower bound (CRLB)[1,2] and related higher-order tensor terms,[3–5] still require environmental pressure derivatives. Whenever actual acoustic data are available to be compared with a model output, environmental pressure derivatives can also be used to compute the gradient of the local error surface.

Environmental pressure derivatives are typically estimated using a finite-difference numerical scheme involving small environmental perturbations, which can lead to stability and convergence problems. An alternate approach that has been often employed in the control theory,[6] geophysics,[7–11] and physical oceanography,[12] literature is the ''adjoint'' or ''costate'' Green's function technique. Several independent derivations of this method[9–11] have shown that by solving two forward problems in the same propagation environment, the environmental pressure derivative with respect to an environmental perturbation can be derived by spatially correlating the two solutions over all space, weighted by the environmental perturbation. The resulting formulas are very similar to those used in diffraction tomography.[13,14]

The application of these expressions to acoustic propagation in a waveguide has been fairly recent.[15] Adjoint parabolic equation (PE) models have been used to estimate the environmental pressure derivatives of two-dimensional refractive index perturbations in a vertical plane connecting an acoustic source and receiver.[16,17] More recently, a normal-mode formulation of the acoustic pressure field was combined with adjoint techniques to derive analytical expressions for first- through third-order environmental pressure derivatives of laterally homogeneous (depth-dependent only) sound speed and density perturbations in a laterally homogeneous waveguide.[18]

In Sec. II the adjoint normal-mode formulation introduced in Ref. 18 is extended to incorporate environmental pressure derivatives with respect to an arbitrary three-dimensional perturbation in a laterally homogeneous waveguide, a situation that would normally require finite-difference computations of a three-dimensional coupled mode or parabolic equation code. The contribution of the paper is to illustrate how, for the restricted geometry of an acoustic waveguide, the three-dimensional spatial integration required by the adjoint method can be analytically simplified into a bounded two-dimensional integral, which can be evaluated numerically with relatively coarse grid sizes. The simplification is attained by using a normal-mode formulation for the Green's function, related in spirit to recent work on a Born scatterer in a waveguide.[15]

To illustrate one application of these formulas, Sec. III

[a)]Portions of this work have been presented at the Oceans 2003 Conference in San Diego, CA.
[b)]Electronic mail: thode@mpl.ucsd.edu

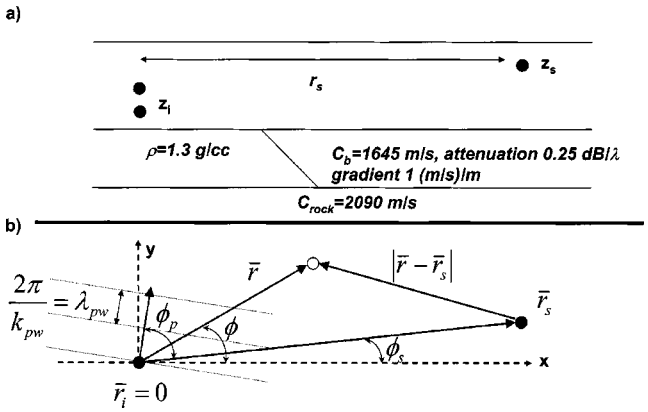

FIG. 1. Geometry used to illustrate adjoint formulas. (a) A 48-element vertical array, with 2-m spacing and first element at 1-m depth, is positioned in a 100-m isovelocity waveguide with bottom speed of 1645 m/s, bottom speed gradient of 1 m/s per m, density 1.3 g/cc, and attenuation of 0.25 dB/wavelength. A rock half-space lies 100 m below the sediment/water interface, with compressional speed of 2090 m/s. The acoustic source is positioned at 3-km horizontal range at 50-m depth. The bottom density is uniform in both the sediment and half-space. (b) View of geometry looking down onto the ocean. The receiver is placed at the coordinate origin. An example of a horizontal plane wave with wave number k_{pw} and propagation azimuth ϕ_p is shown.

presents a simple sensitivity study of horizontal refraction effects produced by plane-wave and compact cylindrical perturbations. A body of literature extending over two decades has examined the issue of horizontal refraction through eddies[19–22] and other features[23–25] in detail; the motivation of Sec. III is not to extend these studies, but to illustrate how the formulas derived here can quickly identify situations where horizontal refraction might be a non-negligible issue, given a particular source/receiver geometry. The first example presented here uses horizontally propagating plane waves as a simple model for internal waves, while the second example uses compact vertical cylindrical perturbations as a model for small eddies or gyres.

II. THEORY

A. General adjoint expression for environmental derivative

Density perturbations are not discussed in this particular paper, but their incorporation should follow similar lines of development as below. However, the spatial gradient of the Green's function would be required as well as the Green's function itself.[18]

A Green's function $g(\bar{r},\bar{r}_s,\omega)$ describes an acoustic field of frequency ω generated at location $\bar{r}_s$ that propagates through an unknown environment to location $\bar{r}$. The explicit dependence of g on frequency is now dropped. The source and receiver positions are expressed in terms of cylindrical coordinates, with the receivers r_i lying on the origin, and the source placed along the x axis, so that $\phi_s = 0$ (Fig. 1). The propagation of the field is governed by the density-dependent inhomogeneous Helmholtz equation

$$\rho(\bar{r})\nabla\cdot\left(\frac{1}{\rho(\bar{r})}\nabla g(\bar{r},\bar{r}_s)\right) + k_{\text{ref}}^2\eta(\bar{r})g(\bar{r},\bar{r}_s) = -\delta(\bar{r}-\bar{r}_s). \tag{1}$$

Here, k_{ref} is a spatially invariant reference medium wave number, and $\eta(\bar{r},\omega)\equiv k(\mathbf{r})^2/k_{\text{ref}}^2 = c_{\text{ref}}^2/c(\mathbf{r})^2$ is the spatially dependent refractive index squared that, along with the spatially dependent density $\rho(\bar{r})$, defines the propagation environment. The linear operator L_0 provides a shorthand way of writing this differential equation.

This refractive-index term can be written as the sum of a laterally homogeneous (but potentially depth-dependent) "background" square refractive index η_0, and a perturbative expansion based on an *infinitesimal* nondimensional sound-speed perturbation magnitude ε

$$\eta(\bar{r}) \equiv \eta_0(z) + \varepsilon\,\eta_\varepsilon(\bar{r}) + \cdots, \tag{2}$$

where $\varepsilon \equiv \delta c/c_{\text{ref}}$, with δc being a compressional sound-speed magnitude in (m/s). The quantity $\eta_\varepsilon \equiv \partial\eta/\partial\varepsilon|_{\varepsilon=0}$ is an order-one term in the perturbative expansion, and represents the derivative of a three-dimensional square index of refraction distribution with respect to the sound-speed perturbation magnitude, and will be subsequently referred to as the "refractive index derivative." If the functional dependence of the square-refractive index is such that higher-order derivatives are both physically relevant and non-negligible, Eq. (2) can be expanded to higher-order terms.

The Green's function $g(\bar{r},\bar{r}_s)$ of the perturbed environment can be expressed as a similar expansion

$$g(\bar{r},\bar{r}_s) \equiv g_0(\bar{r},\bar{r}_s) + \varepsilon g_\varepsilon + \cdots. \tag{3}$$

Here, $g_\varepsilon \equiv \partial g/\partial\varepsilon|_{\varepsilon=0}$ is the derivative of the Green's function with respect to the environmental parameter magnitude, and is assumed to be of order one in this series solution as well. Having expressed the new Green's function as an expansion of the nondimensional ε, a solution can now be found for the Green's function derivative g_ε. The final derivative formula can then be expressed in terms of the dimensional differential δc.

A rigorous derivation of how g_ε can be linearly related to η_ε is reviewed elsewhere,[7,9,11,18] however, a brief heuristic argument can be derived from the Born approximation[14,15]

$$g(\bar{r}_i,\bar{r}_s) \approx g_0(\bar{r}_i,\bar{r}_s) + k_{\text{ref}}^2\rho(\bar{r}_i) \times \int\int\int_V \left[\{\varepsilon\,\eta_\varepsilon(\bar{r})\}\frac{g_0(\bar{r},\bar{r}_i)}{\rho(\bar{r})}g_0(\bar{r},\bar{r}_s)\right]\mathbf{d}^3\mathbf{r}. \tag{4}$$

By rearranging this expression, dividing by ε, and taking the limit as $\varepsilon\to 0$, the approximate equality of Eq. (4) converges to an *exact* solution, which, when multiplied by a appropriate source strength and converted to dimensional units, becomes the acoustic adjoint equation for the derivative of acoustic pressure with respect to compressional speed magnitude

$$\frac{\partial p(\bar{r}_i,\bar{r}_s)}{\partial c} = \left(\frac{S}{S_0}\right)S_0 k_{\text{ref}}^2\rho(\bar{r}_i) \times \int\int\int_V \left[\eta_c(\bar{r})\frac{g(\bar{r},\bar{r}_i)}{\rho(\bar{r})}g(\bar{r},\bar{r}_s)\right]\mathbf{d}^3\mathbf{r}. \tag{5}$$

Here, $S_0=\rho\omega^2 V_0$, with V_0 being a volume injection sufficient to generate a pressure level of 1 Pa at 1 m range (120 dB re: 1 μPa @ 1 m source level). This choice of V_0 sets $S_0=1$ Pa-m, while S is the actual source level of the pressure field in Pa-m. From Eq. (5) onwards the environmental pressure derivative will be written with respect to sound-speed magnitude in dimensional units of m/s, and the zero subscript for the unperturbed Green's function is dropped, with the understanding that the term ''Green's function'' in subsequent discussion will always refer to the *unperturbed* Green's function.

Two comments must be made concerning the validity and practicality of Eq. (5). First, even though it was derived via the Born approximation, Eq. (5) is an *exact* expression for the environmental derivative, as more complete derivations demonstrate. However, if a *finite* perturbation changes the sound-speed magnitude by an amount δc, Eq. (5) can only provide an *approximate* estimate of the perturbed pressure field, in the form of $p(\bar{r}_i,\bar{r}_s)\approx p_0(\bar{r}_i,\bar{r}_s)+\delta c([\partial p(\bar{r}_i,\bar{r}_s)]/\partial c)$, and only if δc is extremely small. Thus, Eq. (5) would be of limited use for full-field inversion procedures, without further information about higher-order derivatives of p like $p_{cc}\equiv\partial^2 p/\partial c^2|_{\varepsilon=0}$, which can be shown to correspond to higher-order terms in the Born approximation.[7]

Second, while the adjoint expression in Eq. (5) does not require a finite differencing scheme, it does so at the cost of requiring a spatial integration of the Green's functions, which must be performed numerically under general geometries, e.g., Ref 8. Without further simplification the evaluation of Eq. (5) faces the same issues with computational speed and convergence as finite-difference approaches. The key result of this paper is that the particular geometry of a laterally homogeneous waveguide permits this integration to be reduced analytically to a numerically stable two-dimensional intergal over azimuth and depth. Furthermore, it will be shown how an appropriate choice of refractive index basis functions permits one to compute a large number of environmental derivatives with only a single set of computations.

B. Orthogonal decomposition of refractive index perturbation

A standard technique in linear inversion theory is to model perturbations as a linear sum of basis functions,[26] i.e., $\eta_c(\bar{r})=\Sigma_p a_p \eta_p(\bar{r})$.

In a similar spirit, in cylindrical coordinates the refractive index derivative can be expressed as a sum of a set of orthogonal basis functions, exploiting an orthogonality relationship between Bessel functions of the first kind J_ν

$$\eta_c(\bar{r},z)=\sum_{q=1}^{Q}\eta_q(z)\sum_{\nu=-\infty}^{\infty}e^{-i\nu\phi}\times\int_0^\infty a(k_p,\nu,q)J_\nu(k_p r)k_p\,dk_p, \tag{6a}$$

with

$$a(k_p,\nu,q)\equiv a_{pq\nu}=\frac{1}{2\pi}\int_0^{2\pi}e^{i\nu\phi}d\phi\times\int_0^\infty dz\int_0^\infty\eta_c(\bar{r},z)\,\eta_q(z)J_\nu(k_p r)r\,dr. \tag{6b}$$

Here, J_ν is a Bessel function of the first kind of order ν. The functions η_q are a set of Q orthonormal vertical basis functions, such as sine and cosine waves, empirical orthogonal functions (EOFs) derived directly from data, acoustic normal modes, or even internal wave modal functions.[27]

Equation (6) suggests that if a set of ''fundamental'' basis functions

$$\eta_{pq\nu}(\bar{r},z)=\eta_q(z)e^{-i\nu\phi}J_\nu(k_p|r|), \tag{7}$$

is inserted into Eq. (5) for $\eta_\varepsilon(\bar{r})$ and evaluated, the result would provide a general solution for the environmental pressure derivative

$$\frac{\partial g(\bar{r}_i,\bar{r}_s)}{\partial c}=\sum_{q=1}^{Q}\sum_{\nu=-\infty}^{\infty}\int_0^\infty a_{p\nu q}\frac{\partial g(\bar{r}_i,\bar{r}_s)}{\partial c_{pq\nu}}k_p\,dk_p$$
$$\frac{\partial g(\bar{r}_i,\bar{r}_s)}{\partial c_{pq\nu}}\equiv\left(\frac{S}{S_0}\right)S_0k_{\mathrm{ref}}^2\rho(\bar{r}_i)\int_V\int\int\left[\eta_q(z)e^{-i\nu\phi}J_\nu(k_p r)\times\frac{g(\bar{r},\bar{r}_i)}{\rho(\bar{r})}g(\bar{r},\bar{r}_s)\right]\mathbf{d}^3\mathbf{r}. \tag{8}$$

For the special case of the horizontally propagating complex plane wave illustrated in Fig. 1(b), with horizontal wave number k_{pw} and propagation direction ϕ_p with respect to the x axis, the basis function decomposition has the form

$$e^{-i\bar{k}_{pw}\cdot\bar{r}}=e^{-ik_{pw}r\cos(\phi-\phi_p)}=\sum_{\nu=0}^{\infty}\beta_\nu(-i)^\nu\cos[\nu(\phi-\phi_p)]J_\nu(k_{pw}r), \tag{9}$$

where $\beta_\nu=2$, except for $\beta_0=1$. Thus, from Eq. (6b)

$$a_{pq\nu}=(-i)^\nu e^{i\nu\phi_p}\frac{\delta(k_{pw}-k_p)}{k_p}\int_0^\infty\eta_q(z)dz, \tag{10}$$

and Eq. (8) becomes

$$\frac{\partial g(\bar{r}_i,\bar{r}_s)}{\partial c_{\text{plane-wave}}}=\sum_{q=1}^{Q}\int_0^\infty\eta_q(z)dz\times\sum_{\nu=-\infty}^{\infty}(-i)^\nu e^{i\nu\phi_p}\frac{\partial g(\bar{r}_i,\bar{r}_s)}{\partial c_{(k_{pw})q\nu}}. \tag{11}$$

All the examples shown in this paper use a single vertical basis function, so Q is restricted to 1.

C. Adjoint solution for basis function in a constant-depth waveguide

Solving the adjoint Eq. (8) requires two Green's functions, one describing propagation from the source r_s to an arbitrary point r, and one describing propagation from the receiver r_i to the same point r [see Fig. 1(b)].

In the geophysics community the Green's functions are typically computed numerically over a set of grid points, and the subsequent spatial correlation is achieved by numerical integration over the grid. Because of computational costs the numerical integration is often restricted to a 2D plane incorporating the source and receiver.[8,28] However, for the case of a laterally homogeneous waveguide the Green's function can be expressed as a sum of normal modes $U_n(z)$, which permits some analytical simplification. To begin, the Green's function between a location r and receiver location centered at the origin is

$$g(\overline{r,r_i})=\frac{i}{4\rho(z_i)}\sum_f U_f(z)U_f(z_i)H_0^{(1)}(k_{rf}|\overline{r}|), \tag{12}$$

and the Green's function between the source at r_s and location r is

$$\begin{aligned} g(\overline{r,r_s}) &= \frac{i}{4\rho(z_s)}\sum_g U_g(z)U_g(z_s)H_0^{(1)}(k_{rg}|\overline{r_s}-\overline{r}|) \\ &= \frac{i}{4\rho(z_s)}\sum_g \sum_{\nu'=0}^{\infty}\beta_{\nu'}U_g(z)U_g(z_s)\cos\nu'(\phi-\phi_s) \\ &\quad\times\begin{cases} J_{\nu'}(k_{rg}\overline{r})H_{\nu'}^{(1)}(k_{rg}\overline{r_s}), & |r|<|r_s| \\ J_{\nu'}(k_{rg}\overline{r_s})H_{\nu'}^{(1)}(k_{rg}\overline{r}), & |r|>|r_s| \end{cases}, \end{aligned} \tag{13}$$

where $H_\nu^{(1)}$ is the νth-order outgoing Hankel function of the first kind. In the second line of Eq. (13), Graf's addition theorem for Bessel functions has been used.[29] Combining Eqs. (7), (12), and (13) into Eq. (8) and performing the azimuthal integration yields nonzero terms only when $\nu'=\pm\nu$.

The final result expresses the environmental pressure derivative as a sum of one-dimensional depth integrals

$$\begin{aligned} \frac{\partial p(\overline{r_i},\overline{r_s})}{\partial a_{pq\nu}} &= \left(\frac{S}{S_0}\right)\left[\frac{-S_0\pi}{8\rho(z_s)}\sum_{f,g} Z_{qfg}U_f(z_i)U_g(z_s)\right. \\ &\quad\left.\times\sum_{\nu=-\infty}^{\infty} R_{p\nu fg}(r_s)e^{-i\nu\phi_s}\right], \end{aligned} \tag{14}$$

$$Z_{qfg}\equiv k_{\mathrm{ref}}^2\int_0^\infty\frac{\eta_q(z')}{\rho_0(z')}U_f(z')U_g(z')dz', \tag{15}$$

$$R_{p\nu fg}(r_s) = \begin{cases} H_\nu^{(1)}(k_{rg}r_s)\displaystyle\int_0^{r_s} rJ_\nu(k_pr)J_\nu(k_{rg}r)H_0^{(1)}(k_{rf}r)dr \\ +J_\nu(k_{rg}r_s)\displaystyle\int_{r_s}^{\infty} rJ_\nu(k_pr)H_\nu^{(1)}(k_{rg}r)H_0^{(1)}(k_{rf}r)dr \end{cases}. \tag{16}$$

Note that while Eq. (15) is symmetric with respect to f and g, Eq. (16) is *not*. The first term of Eq. (16) represents contributions to the spatial correlation from regions where $|r|<|r_s|$, while the second term represents contributions from spatial regions where $|r|>|r_s|$; i.e., a "backscattering" regime.

This integral is highly oscillatory, and the large-argument asymptotic expressions for the Bessel functions cannot be used, because they are only valid whenever $k_{rg}r\gg\nu$. However, Eq. (16) can be simplified in a manner analogous to previous work modeling ocean ambient noise in range-dependent environments.[30] First, note that the triple product within the integrand can be reduced to a two-term integrand using a Bessel addition theorem

$$J_\nu(k_pr)B_\nu(k_{rg}r)=\frac{1}{\pi}\int_0^\pi d\phi B_0(k_{rpg}r)\cos\nu\phi, \tag{17a}$$

$$k_{rpg}^2=k_{rg}^2+k_p^2-2k_{rg}k_p\cos\phi, \tag{17b}$$

where B_ν is either J_ν or $H_\nu^{(1)}$. The range integral can then be solved

$$\begin{aligned} \int_0^{r_s} rJ_0(k_{rpg}r)H_0^{(1)}(k_{rf}r_s)dr &= \frac{k_{rpg}r_sH_0^{(1)}(k_{rf}r_s)J_1(k_{rpg}r_s)-k_{rf}r_sH_1^{(1)}(k_{rf}r_s)J_0(k_{rpg}r_s)-2i/\pi}{k_{rpg}^2-k_{rf}^2}, \\ \int_{r_s}^{\infty} rH_0^{(1)}(k_{rpg}r)H_0^{(1)}(k_{rf}r_s)dr &= -\frac{k_{rpg}r_sH_0^{(1)}(k_{rf}r_s)H_1^{(1)}(k_{rpg}r_s)-k_{rf}r_sH_1^{(1)}(k_{rf}r_s)H_0^{(1)}(k_{rpg}r_s)}{k_{rpg}^2-k_{rf}^2}. \end{aligned} \tag{18}$$

The constant $2i/\pi$ arises from evaluating the limit at $r=0$, using the small argument approximations for $H_1^{(1)}$ and J_0. Since k_p is always real and k_{rg} and k_{rf} will have imaginary components due to bottom attenuation, the upper limit of the integral will always vanish, and the denominator of (18) will always be nonzero.

Combining Eqs. (16)–(18) creates a numerically stable bounded integral that can be solved with a relatively coarse integration step

$$R_{p\nu fg}(r_s)=\frac{r_s}{\pi}\int_0^\pi\frac{\cos[\nu\phi]d\phi}{k_{rpg}^2-k_{rf}^2}\begin{Bmatrix} k_{rpg}H_0^{(1)}(k_{rf}r_s)[H_\nu^{(1)}(k_{rg}r_s)J_1(k_{rpg}r_s)-H_1^{(1)}(k_{rpg}r_s)J_\nu(k_{rg}r_s)] \\ -k_{rf}H_1^{(1)}(k_{rf}r_s)[H_\nu^{(1)}(k_{rg}r_s)J_0(k_{rpg}r_s)-H_0^{(1)}(k_{rpg}r_s)J_\nu(k_{rg}r_s)] \\ -2iH_\nu^{(1)}(k_{rg}r_s)/\pi \end{Bmatrix}. \tag{19}$$

For the special case $k_p=0$ (range-independent perturbation), all azimuthal terms vanish except for $\nu=0$, and $R_{p\nu fg}$ reduces to a form similar to that obtained in Ref. 18

$$R_{00fg}(r_s)=\begin{cases} -\dfrac{2i}{\pi}\dfrac{H_0^{(1)}(k_{rf}r_s)-H_0^{(1)}(k_{rg}r_s)}{k_{rf}^2-k_{rg}^2} & f\neq g \\ \dfrac{ir_sH_1^{(1)}(k_{rf}r_s)}{\pi k_{rf}} & f=g \end{cases}. \tag{20}$$

Equation (19) requires a numerical integration over ϕ for each basis function desired. Practically it was found that the integrand need only be evaluated at around 1000 pts to achieve the needed precision. While the form of Eq. (19) may be intuitively unenlightening, substituting the large-argument asymptotic expansions for the Bessel functions indicates that the integral should produce large values whenever $k_p=k_{rf}\pm k_{rg}$, an observation that is verified in the following section.

Note that $R_{p\nu fg}$ is unequal to $R_{p\nu gf}$; i.e., switching the source and receiver does not produce the same environmental derivative, i.e., reciprocity does not hold. The reason for this asymmetry is that the perturbation origin of Eqs. (12) and (13) has been changed. Thus, swapping source and receiver creates a situation where the basis functions are centered at the source, and not the receiver, as in the original problem.

III. NUMERICAL EXAMPLES

A. Modeled waveguide environment

Here, Eqs. (14), (15), and (19) are demonstrated in a sensitivity study using a simple waveguide environment. An omnidirectional 20-Hz source is placed in a isovelocity waveguide 100 m deep, with a bottom speed of 1645 m/s, and standard values for a linear bottom gradient, density, and attenuation (Fig. 1, caption). A bottom half-space with a compressional speed of 2090 m/s begins 100 m below the water/sediment interface. At 20 Hz this waveguide supports six propagating modes. The source/receiver separation in the following examples has been set to either 1 or 3 km, with the source always placed at 50-m depth, and 48 receivers aligned in a vertical array with 2-m spacing.

B. Properties of range integral $R_{p\nu fg}$

The expression in Eq. (19) does not lend itself to physical insight, so Fig. 2 plots the integral as a function of perturbation wave number k_p and ν, using values of k_{rf} and k_{rg} computed from the environment presented above. In the top subplot $k_{rf}=k_{rg}$, and in the bottom subplot they are different. While the numerical computation of Eq. (19) is straightforward, some numerical instability issues arise for large orders of ν. While an asymptotic expansion of Eq. (19) for high-order ν demonstrates that the integral must converge to zero as ν grows large, the numerical evaluation becomes unstable and diverges from zero whenever $\nu>k_{rf}|r_s|$. Therefore, in all computations presented here $R_{p\nu fg}$ is set to zero whenever ν satisfies the above inequality.

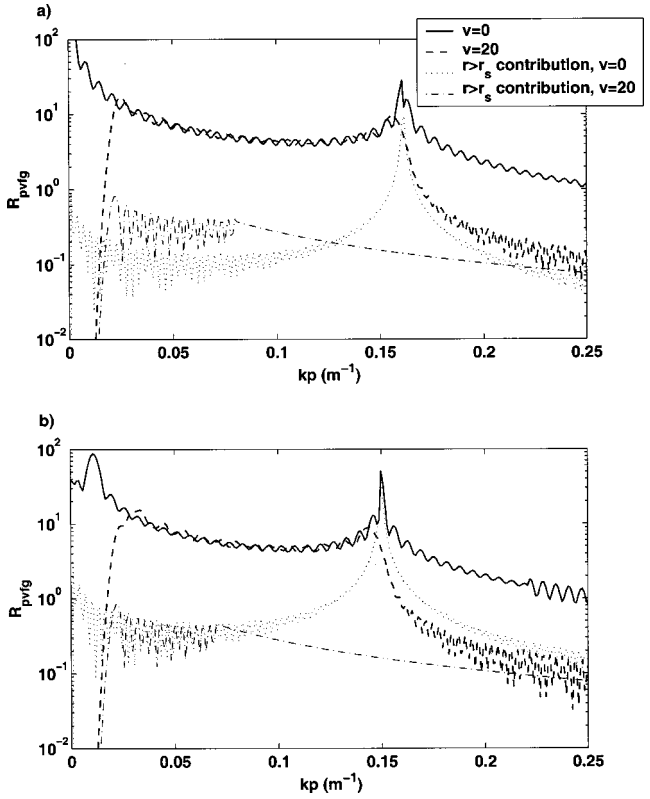

FIG. 2. Plot of $R_{p\nu fg}$ as a function of perturbation wavelength k_p and azimuthal index ν, using modal wave numbers computed from the environment described in Fig. 1, and for a source/receiver separation of 1 km. Solid line: $\nu=0$ (azimuthally symmetric case), dashed line, $\nu=20$. Dotted line: contribution of second term of Eq. (15) for $\nu=0$, where $r>r_s$. Dash-dot line: contribution of second term when $\nu=20$. (a) $k_{rf}=k_{rg}=0.0806$; (b) $k_{rf}=0.0806$, $k_{rg}=0.069\,392$.

The most obvious feature of both Figs. 2(a) and (b) is that $R_{p\nu fg}$ only has significant values whenever $k_{rf}-k_{rg}<k_p<k_{rf}+k_{rg}$. Since $k_{rf}\sim k_{\mathrm{ref}}$, the medium wave number, one can conclude that the propagating acoustic field is only sensitive to perturbation spatial wavelengths that are larger than half of the medium acoustic wavelength, a result well-known from diffraction tomography,[14,31] a procedure that also makes extensive use of the Born approximation. For the case of an azimuthally symmetric perturbation component ($\nu=0$), one sees that whenever k_p is equal to the sum or difference of a set of horizontal wave numbers, $R_{p\nu fg}$ attains a peak, indicating that a propagating acoustic field is especially sensitive to perturbation components with a spatial wave number that matches the sum or differences of pairs of modal wave numbers. Azimuthally dependent perturbation components ($\nu>0$) also display similar peaks, but they occur at slightly different perturbation wave numbers, as can be seen for the case of $\nu=20$ in Fig. 2. The peak associated with the difference between modal wave numbers migrates to a k_p slightly greater than $k_{rf}-k_{rg}$, while the peak associated with the sum of modal wave numbers shifts to a value slightly lower than $k_{rf}+k_{rg}$.

As the range separation r_s between source and receiver increases, these peaks become larger and narrower, indicating that at large ranges and for azisymmetric perturbations, the acoustic field becomes sensitive only to perturbation

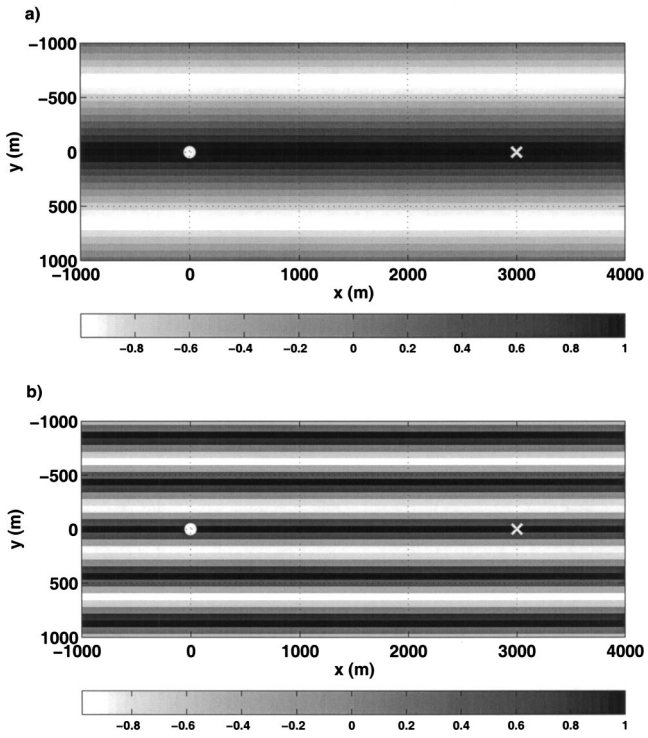

FIG. 3. Examples of plane-wave perturbations that yield the same two-dimensional range–depth perturbation in the vertical plane between acoustic source and receiver. The white circle marks the receiving array location, while the white cross marks the source location at 3-km horizontal range: (a) 1.28-km wavelength perturbation oriented along the y axis ($\phi_p = 90°$); (b) 426-m wavelength perturbation oriented along the y axis.

wavelengths quantized at $k_{rf} \pm k_{rg}$, a result obtained independently by another analysis.[15] It is also interesting to separate the integral contributions into the first and second terms visible in Eq. (16). Whenever $\nu = 0$ contributions from regions where $r > r_s$ (''backscatter region'') cannot be neglected, but for $\nu > 0$ this upper range integral contributions become relatively small—i.e., 10% of the amplitude at the peak in the figure shown.

C. Effect of a horizontal plane-wave perturbation on pressure derivative

As suggested by Eq. (11), it should be straightforward to compute the environmental pressure derivative with respect to horizontally propagating plane wave. As illustrated in Fig. 1(b), one simply evaluates Eqs. (14)–(15) and (19) for $k_p = k_{pw}$ and $\phi_s = \phi_p$, for all values of ν up to $\nu_{\max} = k_{rf} r_s$. The results can then be combined via Eq. (11).

In this section a set of horizontally propagating three-dimensional plane waves has been computed, each one with the same values along the vertical cross section connecting the source and receiver shown in Fig. 1(a), for a source–range separation of 3 km. Two examples of these perturbations are plotted in Fig. 3, looking down onto the ocean surface from above. Two types of depth dependence are modeled: one where the perturbation has a constant value in the water column, and is zero in the ocean bottom, and one where the perturbation has a constant value in the ocean bottom, but is zero in the ocean column. In other words, the horizontal cross sections visible in Fig. 3 would have the same appearance if cut across a different depth, provided that depth is in the same medium (water or ocean bottom).

These perturbations are cosine waves with $\phi_p = 90°$. Therefore, the perturbation values in the vertical plane between the source and receiver are always unity, a situation that was checked via numerical synthesis of the perturbations. This particular perturbation set thus provides a simple opportunity to explore the circumstances under which perturbation components from outside the vertical plane connecting the source and receiver cannot be neglected. In other words, at what perturbation wavelength scale do horizontal refraction effects become non-negligible?

Figure 4 illustrates the magnitude and phase of the environmental pressure derivative across the vertical receiving array as a function of the plane-wave perturbation number k_{pw}, for the case where the perturbation exists only in the water column. A perturbation wave number of 0 indicates a

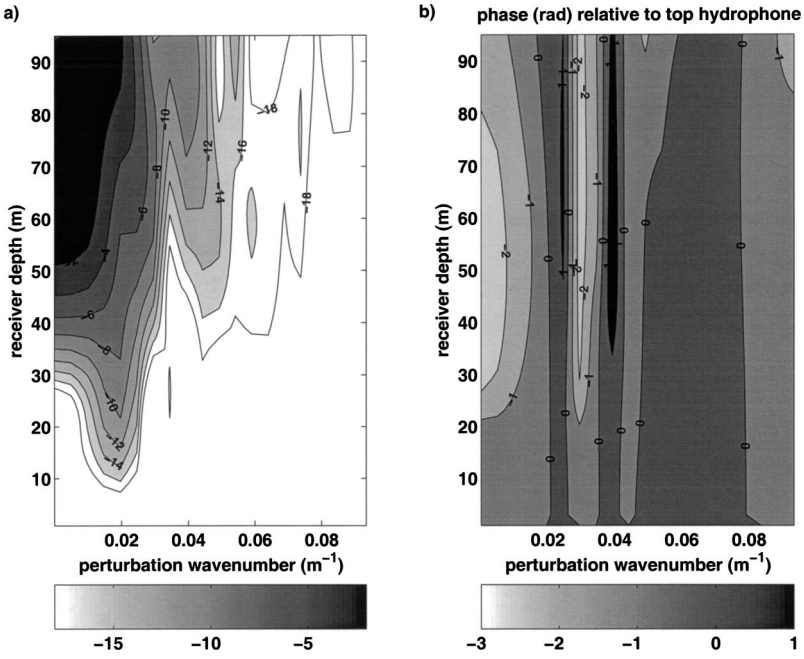

FIG. 4. Effect of plane-wave water-column perturbations on environmental pressure derivative for a 20-Hz field with source level of 120 dB re: 1 μPa @ 1 m, derived from source and receiver geometries shown in Figs. 1 and 3. All perturbations would appear identical in a 2D range–depth slice between source and receiver array. (a) Magnitude in dB of pressure derivative as a function of receiving element depth and perturbation wave number, relative to the maximum environmental pressure derivative of 1.12×10^{-7} Pa/(m/s) attained by the azimuthally symmetric (''range-independent'') result at the x-axis origin. The right limit of the x axis corresponds to a 62-m wavelength. (b) Phase of the environmental derivative, relative to the top receiving hydrophone, as a function of perturbation wave number.

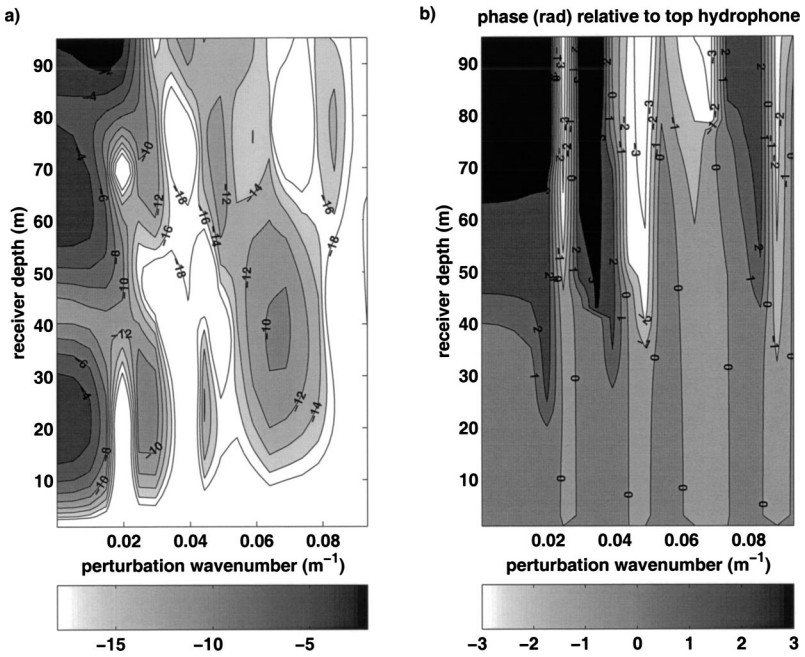

FIG. 5. Same as Fig. 4, but with the plane-wave perturbation restricted to the bottom half-space. Environmental derivative magnitude is displayed in dB relative to the maximum environmental pressure derivative of 6.31×10^{-8} Pa/(m/s).

constant perturbation value over all space (range-independent perturbation). For large wavelengths (small perturbation wave numbers) the environmental pressure derivative is very similar to the range-independent case, but starting at perturbation wavelengths of about 400 m (5 wavelengths of a 20-Hz signal) the phase and magnitude of the derivative change markedly, with a noticeable trend to smaller magnitudes at higher perturbation wavelengths. Figure 5 illustrates a similar computation, but with the perturbation restricted to the ocean bottom. A similar result is seen, in that the environmental pressure derivative changes markedly once the perturbation wavelength decreases below 400 m. An actual plane-wave ocean perturbation, such as those generated by internal waves,[27] would not generate a uniform perturbation with depth, but is generally restricted to a certain portion of the water column. Thus, the horizontal refraction effects produced by realistic plane-wave perturbations, which would be a simple extension of the computations shown here, may not be as large.

D. Effect of a compact cylindrical perturbation on pressure derivative

A second three-dimensional perturbation that can be evaluated analytically is a vertical cylinder with a circular horizontal cross section, which provides a convenient means for investigating the effect of a localized perturbation on the modal field. The perturbation might be considered a very simple model of an eddy.[19,21,32] The geometry of the cylindrical perturbation is illustrated in Fig. 6, from both a top view (a) and a perspective view (b). As with the plane-wave perturbation, the perturbation can be restricted to the water column, below the ocean bottom, or both.

By exploiting Graf's addition theorem one can derive the basis coefficients [Eq. (6b)] needed to construct a circle with radius a displaced from the receiver origin by a distance r_{shift} and by a rotation angle ϕ_{shift} from the x axis [Fig. 6(a)], for the basis functions in Eq. (7)

$$a_{pq\nu}=\frac{aJ_1(k_pa)}{k_p}J_\nu(k_pr_{\text{shift}})e^{-i\nu\phi_{\text{shift}}}. \tag{21}$$

Thus, once a set of derivatives with respect to a set of basis function perturbations has been computed, it is straightforward to compute environmental derivatives for cylindrical perturbations of various diameters at any location.

To illustrate Eq. (21), two cylindrical perturbations with respective radii of 150 and 600 m were inserted into the waveguide environment of Fig. 1, with 1-km horizontal range between the vertical receiving array and perturbation center, and with the 50-m-deep acoustic source remaining at 3-km range. To approximate the continuous integral implied by Eq. (8), k_p was evaluated at 512 points between 0 and 0.251 m^{-1}, or three times the medium wave number. This sampling provided sufficient spacing between the discrete values of k_p so that any artifacts generated appear at ranges much greater than the source range r_s. A convergence test determined that a value of $\nu=60$ was sufficient to reproduce the perturbation at these ranges.

The question of the sensitivity of the environmental pressure derivative to a localized out-of-plane perturbation

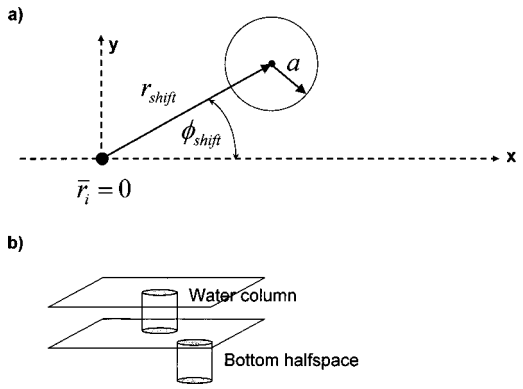

FIG. 6. Geometry of offset cylindrical perturbation: (a) top view; (b) perspective view.

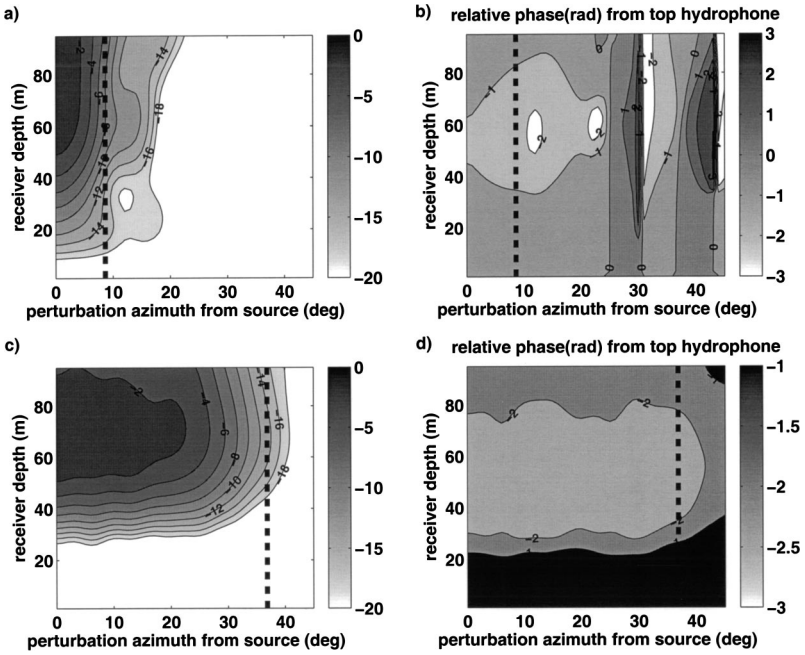

FIG. 7. Effect of a cylindrical (''eddy'') perturbation in water column on 20-Hz acoustic field with source level of 120 dB re: 1 μPa @ 1 m, as a function of perturbation azimuth ϕ_{shift}. The center of the perturbation r_{shift} lies 1 km from the origin. (a) $a=150$-m radius perturbation: environmental pressure derivative magnitude in dB re: the maximum magnitude of 1.58×10^{-8} Pa/(m/s); and (b) relative phase of environmental derivative; (c) $a=600$-m radius perturbation: environmental pressure derivative magnitude in dB re: the maximum magnitude of 7.94×10^{-8} Pa/(m/s) and (d) relative phase.

can be explored by systematically changing the rotation angle ϕ_{shift} in Eq. (21), thus rotating the perturbation around the origin. Beyond some geometric angle $\phi_{\text{extent}}=\sin^{-1}(a/r_{\text{shift}})$ the physical boundaries of the perturbation will no longer intersect the vertical plane intersecting the source and receiver array.

Figures 7 and 8 show a plot similar to Figs. 4 and 5, in that the magnitude and relative phases of the environmental pressure derivative of a 20-Hz signal are shown across the vertical receiving array. This time, however, the horizontal axis represents the rotation angle ϕ_{shift}, and the vertical dashed lines mark ϕ_{extent}. The color map scale has been normalized and plotted on a log scale, so that the maximum magnitude of the environmental pressure derivative across the receiving array when $\phi_{\text{shift}}=0$ has been defined as 0 dB. This value will be subsequently referred to as the ''in-plane maximum.''

Figure 7 shows the effect of a cylindrical perturbation placed in the water column only, with the top row showing the effect of the 150-m radius perturbation, and the bottom row the effect of the 600-m perturbation. The figures show that the environmental pressure derivative still exists even when the perturbations lie completely outside the vertical source–receiver plane ($\phi_{\text{shift}}>\phi_{\text{extent}}$), but with a magnitude at least 8 dB less than the in-plane maximum. The smaller the perturbation radius, the larger the relative magnitudes the out-of-plane results tend to be. This observation is consistent with the expectation that the greater curvature of small-radii perturbations should have relatively larger horizontal refraction effects.

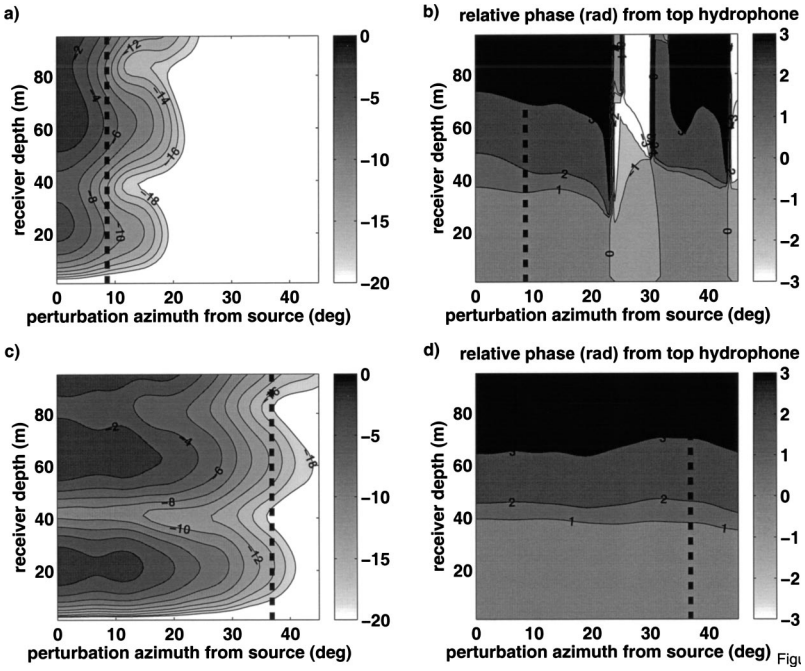

FIG. 8. Effect of cylindrical perturbation in ocean bottom on 20-Hz acoustic field, as a function of ϕ_{shift}, for $r_{\text{shift}}=1$ km. (a) $a=150$-m radius perturbation: environmental pressure derivative magnitude in dB re: the maximum magnitude of 6.31×10^{-9} Pa/(m/s); and (b) relative phase of environmental derivative; (c) $a=600$-m radius perturbation: environmental pressure derivative magnitude in dB re: the maximum magnitude of 2.24×10^{-8} Pa/(m/s) and (d) relative phase.

Figure 8 shows an identical situation, except with the cylindrical perturbations existing only beneath the ocean bottom. As with Fig. 7, derivatives with respect to out-of-plane perturbations exist, with larger relative magnitudes produced by perturbations with smaller radii. Furthermore, the out-of-plane results can be non-negligible when compared with the in-plane maximum. For example, in subplot (a) a 150-m radius perturbation produces environmental pressure derivatives that are within 10 dB of the in-plane maximum out to rotation angles of 15 deg, if the receiver depth is 50 m. This angle is nearly twice the value of ϕ_{extent}.

The results of this simple sensitivity study on this particular deployment configuration indicate that while neglecting out-of-plane refraction effects may be a safe assumption for certain cylindrical perturbations in the water column, it may not be a valid assumption for small-radii perturbations in the ocean bottom.

As the environmental pressure field can be interpreted as a field ''scattered'' from an infinitesimal perturbation via the Born approximation, some further physical insight into these results can be obtained by computing how an incident acoustic plane wave diffracts from an aperture with the same lateral dimensions as the perturbation.[33,34] As a normal mode consists of two plane waves propagating nearly horizontally, the assumption of an incident plane wave in the diffraction analysis is valid. For a perturbation radius of 600 m, a point 2-km range from the perturbation center lies within the Fresnel diffraction region ($r \approx a^{1/3}\sqrt{ka/2} = 1700\,\text{m}$).[14] Treating the perturbation as a rectangular aperture 1.2 km wide, an analysis of the resulting Fresnel diffraction pattern using a Cornu spiral finds that the boundaries of the geometric shadow are quite sharp. Thus, for the 600-m radius perturbation the apparent angular half-width of the diffracted field would be very close to the geometric half-width of 36° for ϕ_{extent} at this range, as was found to be the case.

By contrast, a perturbation radius of 150 m places the 2-km range receiver location in the Fraunhofer region ($r > 4a^2/\lambda = 1200\,\text{m}$), and diffraction effects are found to be prominent. Given a total perturbation ''aperture'' of 300 m, the azimuthal angle at which the diffraction mainlobe attains its first null is $\phi_{\text{null}} = \lambda/2a = 14.4°$ from the mainlobe center, close to the angular extent of the observed pressure derivatives in Figs. 7(a) and 8(a), and nearly twice as large as the geometrical angle ϕ_{extent}. Thus, the predictions of simple plane-wave diffraction theory are consistent with the results from the expressions derived here.

IV. CONCLUSION

A semianalytic set of expressions has been derived for the derivative of an acoustic pressure field in a laterally homogeneous waveguide, with respect to an arbitrary three-dimensional refractive index perturbation anywhere within that waveguide, using a normal-mode formulation. The expressions, which were derived using an adjoint Green's function formalism, require two sets of one-dimensional numerical integrations over a set of spatial basis functions. Once these integrations have been computed, a wide variety of perturbations can be rapidly synthesized. The extension of these expressions to density perturbations, although not presented here, should follow a similar route, although the spatial gradient of the Green's function, and thus the gradient of Eqs. (12) and (13), would be required.[18]

These expressions have been demonstrated in simple sensitivity studies that illustrate how both plane-wave and cylindrical perturbations can influence the received pressure field, even when the perturbation does not physically intersect the vertical plane connecting the source and receiver. Whether realistic ocean perturbations produce similar out-of-plane effects has been a question of practical interest.[19,23–25,35,36] Many realistic perturbations, especially those of internal linear waves,[27] can be expressed as straightforward combinations of the basis functions of Eq. (7), so these expressions may be useful in more sophisticated sensitivity studies.

In practical terms the expressions used here could be used to check whether significant horizontal refraction effects might be expected under various experimental deployment geometries, before applying tomographic algorithms that neglect out-of-plane refraction effects. These expressions might also serve as benchmarks for three-dimensional propagation codes, such as a three-dimensional parabolic equation code.[37,38]

These expressions have some theoretical interest as well, as they can be used to compute the Cramer–Rao bounds for environmental parameters related to three-dimensional structures in an ocean waveguide, a rigorous approach for estimating the sensitivity of an acoustic field to a perturbation. For example, the minimum variance of internal wave spectrum estimates extracted from acoustic data could be derived as a function of input sample size and signal-to-noise ratio.

ACKNOWLEDGMENTS

The author wishes to thank Paul Hursky, Bruce Cornelle, Peter Gerstoft, and Bill Kuperman for helpful discussions on adjoint theory. Michael Buckingham and William Siegmann provided advice and references on Bessel addition theorems and perturbative expansions, respectively, while Peter Gerstoft helped provide references to the geoacoustic inversion literature. The ONR Uncertainty Program [ONR Contract No. N00014-00-F-0395] provided support for the authors of this paper, and the ONR Acoustic Entry-Level Faculty Award [ONR Contract No. N00014-03-1-0215] provided supplemental support.

[1] L. L. Van Trees, *Detection, Estimation and Modulation Theory* (Wiley, New York, 1970).
[2] A. B. Baggeroer, W. A. Kuperman, and H. Schmidt, ''Matched field processing: Source localization in correlated noise as an optimum parameter estimation problem,'' J. Acoust. Soc. Am. **83**, 571–587 (1988).
[3] E. Naftali and N. C. Makris, ''Necessary conditions for a maximum-likelihood estimate to become asymptotically unbiased and attain the Cramer–Rao lower bound. I. General approach with an application to time-delay and Doppler shift estimation,'' J. Acoust. Soc. Am. **110**, 1917–1930 (2001).
[4] A. M. Thode, M. Zanolin, E. Naftali, P. Ratilal, and N. C. Makris, ''Necessary conditions for a maximum likelihood estimate to become asymptotically unbiased and attain the Cramer–Rao lower bound. II. Range and depth localization of a sound source in an ocean waveguide,'' J. Acoust. Soc. Am. **112**, 1890–1910 (2002).
[5] M. Zanolin, I. Ingram, A. M. Thode, and N. C. Makris, ''Asymptotic

accuracy of geoacoustic inversions,'' J. Acoust. Soc. Am. (submitted).
[6] D. E. Kirk, *Optimal Control Theory* (Prentice-Hall, Englewood Cliffs, NJ, 1970).
[7] P. R. McGillivray and D. W. Oldenburg, ''Methods for calculation of Frechet derivatives and sensitivities for the nonlinear inverse problem: A comparative study,'' Geophys. Prospect. **38**, 499–524 (1990).
[8] R. G. Pratt, C. Shin, and G. J. Hicks, ''Gauss–Newton and full Newton methods in frequency-space seismic waveform inversion,'' J. Geophys. Int. **133**, 341–362 (1998).
[9] A. Tarantola, ''Inversion of seismic reflection data in the acoustic approximation,'' Geophysics **49**, 1259–1266 (1984).
[10] M. S. Zhdanov, *Geophysical Inverse Theory and Regularization Problems* (Elsevier, Amsterdam, 2002).
[11] S. J. Norton, ''Iterative inverse scattering algorithms: Methods of computing Frechet derivatives,'' J. Acoust. Soc. Am. **106**, 2653–2660 (1999).
[12] C. Wunsch, *The Ocean Circulation Inverse Problem* (Cambridge University Press, Cambridge, MA, 1996).
[13] R.-S. Wu and M. N. Toksoz, ''Diffraction tomography and multisource holography applied to seismic imaging,'' Geophysics **52**, 11–25 (1987).
[14] M. Born and E. Wolf, *Principles of optics* (Cambridge University Press, Cambridge, 1999).
[15] D. N. G. Roy and G. J. Orris, ''A Born scatterer in an acoustical waveguide,'' J. Acoust. Soc. Am. **114**, 626–633 (2003).
[16] P. Hursky, M. B. Porter, B. Cornuelle, W. S. Hodgkiss, and W. A. Kuperman, ''Adjoint modeling for acoustic inversion,'' J. Acoust. Soc. Am. **115**, 607–619 (2003).
[17] J.-C. L. Gac, Y. Stephan, M. Asch, P. Helluy, and J.-P. Hermand, ''A variational approach for geoacoustic inversion using adjoint modeling of a PE approximation model with nonlocal impedance conditions,'' in *Sixth International Conference on Theoretical and Computational Acoustics*, edited by A. Tolstoy, E.-C. Shang, and Y.-C. Teng (World Scientific, Naval Undersea Warfare Center Division, Singapore, 2003).
[18] A. M. Thode and K. Kim, ''Multiple-order derivatives of a waveguide acoustic field with respect to sound speed, density, and frequency,'' J. Acoust. Soc. Am. (accepted).
[19] R. N. Baer, ''Calculations of sound propagation through an eddy,'' J. Acoust. Soc. Am. **67**, 1180–1185 (1980).
[20] M. V. Hall and M. A. Irving, ''Application of adiabatic mode theory to the calculation of horizontal refraction through a mesoscale ocean eddy,'' J. Acoust. Soc. Am. **86**, 1465–1477 (1989).
[21] W. H. Munk, ''Horizontal deflection of acoustic paths by mesoscale eddies,'' J. Phys. Oceanogr. **10**, 596–604 (1980).
[22] W. H. Munk and F. Zachariasen, ''Refraction of sound by islands and seamounts,'' J. Atmos. Ocean. Technol. **8**, 554–574 (1991).
[23] S. Finette and R. Oba, ''Horizontal array beamforming in an azimuthally anisotropic internal wave field,'' J. Acoust. Soc. Am. **114**, 131–144 (2003).
[24] O. A. Godin, ''A 2D description of sound propagation in a horizontally inhomogeneous ocean,'' J. Comput. Acoust. **10**, 123–151 (2002).
[25] A. Tolstoy, ''3D propagation issues and models,'' J. Comput. Acoust. **4**, 243–271 (1996).
[26] R. L. Parker, *Geophysical Inverse Theory* (Princeton University Press, Princeton, NJ, 1994).
[27] T. C. Yang and K. Yoo, ''Internal wave spectrum in shallow water: Measurement and comparison with Garrett-Munk model,'' IEEE J. Ocean. Eng. **24**, 333–345 (1999).
[28] R. G. Pratt and M. H. Worthington, ''Inverse theory applied to multisource cross-hole tomography. I. Acoustic wave-equation method,'' Geophys. Prospect. **38**, 287–310 (1990).
[29] M. Abramowitz and I. A. Stegun, *Handbook of Mathematical Functions* (Dover, New York, 1972).
[30] J. S. Perkins, W. A. Kuperman, F. Ingenito, L. T. Fialkowski, and J. Glattetre, ''Modeling ambient noise in three-dimensional ocean environments,'' J. Acoust. Soc. Am. **93**, 739–752 (1993).
[31] T.-W. Lo, G. L. Duckworth, and M. N. Toksoz, ''Minimum cross entropy seismic diffraction tomography,'' J. Acoust. Soc. Am. **87**, 748–756 (1990).
[32] R. N. Baer, ''Propagation through a three-dimensional eddy including effects on an array,'' J. Acoust. Soc. Am. **69**, 70–75 (1981).
[33] E. G. Williams, *Fourier Acoustics* (Academic, London, 1999).
[34] J. J. Bowman, T. B. A. Senior, and P. L. E. Uselenghi, *Electromagnetic and Acoustic Scattering by Simple Shapes* (Hemisphere, New York, New York, 1987).
[35] J. C. Preisig and T. F. Duda, ''Coupled acoustic mode propagation through continental-shelf internal solitary waves,'' IEEE J. Ocean. Eng. **22**, 256–269 (1997).
[36] S. Finette, M. H. Orr, A. Turgut, J. R. Apel, J. Badiey, C. S. Chiu, R. H. Headrick, J. N. Kemp, J. F. Lynch, A. E. Newhall, K. von der Heydt, B. Pasewark, S. N. Wolf, and D. Tielbuerger, ''Acoustic field variability induced by time evolving internal wave fields,'' J. Acoust. Soc. Am. **108**, 957–972 (2000).
[37] W. L. Siegmann, G. A. Kriegsmann, and D. Lee, ''A wide-angle three-dimensional parabolic wave equation,'' J. Acoust. Soc. Am. **78**, 659–664 (1985).
[38] K. B. Smith, ''A three-dimensional propagation algorithm using finite azimuthal aperture,'' J. Acoust. Soc. Am. **106**, 3231–3239 (1999).